Research Square

Preprints are preliminary reports that have not undergone peer review.
They should not be considered conclusive, used to inform clinical practice,
or referenced by the media as validated information.

Topological characterization for the geometric origin of transition in electrical conductivity for hybrid nanocomposites

Jungmin Lee
Korea Aerospace University
Sang Hyun Lee
Korea University
Jinyoung Hwang (jinhwang@kau.ac.kr)
Korea Aerospace University

Article

Keywords: Hybrid nanocomposites, Voronoi Tessellation, Swiss cheese model, Percolation theory, Machine learning

Posted Date: April 11th, 2022

DOI: https://doi.org/10.21203/rs.3.rs-1536009/v1

License: This work is licensed under a Creative Commons Attribution 4.0 International License.
Read Full License

Main Manuscript for

Topological characterization for the geometric origin of transition in electrical conductivity for hybrid nanocomposites

Jungmin Lee[a], Sang Hyun Lee[b], Jinyoung Hwang[a,*]

[a]School of Electronics and Information Engineering, Korea Aerospace University, Goyang, 10540;

[b]School of Electrical Engineering, Korea University, Seoul, 02841

Email: jungmin95@kau.kr, sanghyunlee@korea.ac.kr, jinhwang@kau.ac.kr

*To whom correspondence may be addressed. Email: jinhwang@kau.ac.kr

Author Contributions: J. L. and J. H. designed the research; J. L performed the research; J. H. and S. L. analyzed data, J. L., S. L., and J. H. wrote the manuscript.

Availability of Data and Materials: The datasets used and/or analysed during the current study available from the corresponding author on reasonable request.

Competing Interest Statement: The authors declare no competing interest.

Classification: Physical Science, Engineering

Keywords: Hybrid nanocomposites, Voronoi Tessellation, Swiss cheese model, Percolation theory, Machine learning

This PDF file includes:

Main Text
Figures 1 to 7
Tables 1 to 4

Abstract

In this study, the analytical relationship between the electrical conductivity of hybrid nanocomposites consisting of conducting nanowires and insulating particulate fillers was investigated. We measured the performance as a function of the major factors defined by the combination of physical parameters of the constituent fillers. The major factors were identified using data mining techniques. The topological structure of the nanocomposites was described using a combination of Voronoi tessellation and the Swiss cheese model. Based on the geometrical framework, an analytical model of the electrical conductivity of the hybrid nanocomposites was built based on the Kozeny–Carman approach. The model delineates a one-dimensional characterization of the transition in electrical conductivity associated with the size ratio of the fillers and enables to visualize the quantitative relationship between the topological structure and electrical conductivity of the hybrid nanocomposites. Formalism facilitates the design of the physical properties of hybrid nanocomposites before their synthesis.

Introduction

Hybrid nanocomposites are materials fabricated by uniform dispersion of more than two types of fillers over a medium. Multiple types of fillers are mixed in a medium of composite materials to achieve improved performance compared to the performance of single-type nanocomposite materials[1-4] or to reinforce the properties of a primary filler with the support of secondary fillers[5-7]. For example, a hybrid nanocomposite prepared from a mixture of carbon nanotubes (CNTs) and silica particles[8-10] has been used as a flexible conducting material. The concentration of CNTs can control the electrical conductivity of the material; therefore, a high concentration of CNTs is required to achieve highly conductive composites. However, the high production cost of CNTs renders high-concentration CNT composite materials industrially inefficient. To address this drawback, low-priced silica particles have been distributed along the CNTs to achieve enhanced electrical conductivity with the same concentration of CNTs. Therefore, hybrid nanocomposite materials facilitate the delicate control of the desired material properties over natural materials and provide an economic advantage because fewer primary constituent materials are required for nanocomposites.

Hybrid nanocomposites can realize a variety of combined material properties with controlled compositions of multiple types of fillers while forming a complicated microscopic structure of random morphology[11-13]. Such a random structure impairs the accurate prediction and hinders the design of material properties, occasionally resulting in distinct and unexpected material characteristics. In contrast, single-filler nanocomposites have been studied for several accurate characterizations, using statistical and computational methods[14-18]. However, a straightforward combination of individual models associated with component filler materials mixed in hybrid nanocomposites fails to fully characterize the nontrivial aspects of hybrid material

properties. For example, when working with nanocomposite materials with CNTs and silica particles, the addition of silica particles can result in degraded electrical conductivity rather than an improvement[19-25]. Owing to the complicated microscopic structures, most previous studies on the properties of hybrid nanocomposites are limited as they rely on numerical approaches[26-28]. Analytical models have not been appropriately characterized to describe the electrically conductive properties and critical parameters mathematically.

In this study, an analytical model to predict the electrical conductivity of hybrid nanocomposite materials composed of conducting nanowires and insulating particles was developed. This model enables the collection of comprehensive behavioral patterns and tracking of their variations for data analysis. We consider the topological structures of nanowire networks of hybrid nanocomposites in a two-dimensional domain. In practice, the hybrid nanocomposites were prepared in a paste by dispersing the fillers in polymeric or fluidic mediums, and they were spread on the surface in the form of a thin film with a thickness similar to the conducting nanowire length. Therefore, the overall nanowire network can be seen in a two-dimensional surface rather than in a three-dimensional volume.

This work provides the following contributions: 1) A comprehensive numerical evaluation of the electrical conductivity of hybrid nanocomposite materials was performed. Data mining and machine learning techniques were applied to screen the computational results to identify critical factors describing the behavioral patterns of the electrical conductivity of the hybrid nanocomposites. 2) A computational geometric framework for Voronoi tessellation combined with Swiss cheese models is introduced. The Kozeny–Carman approach is applied to the geometrical framework to develop an analytical relationship for the electrical conductivity of the hybrid nanocomposites as

a function of the geometry and content of the constituent fillers. This novel formalism determines the design rules for synthesizing hybrid nanocomposite materials. It defines a quantitative relationship among the physical parameters of the constituent fillers that induce variations in electrical conductivity.

Results

1) Data preprocessing and principal component analysis with the dataset

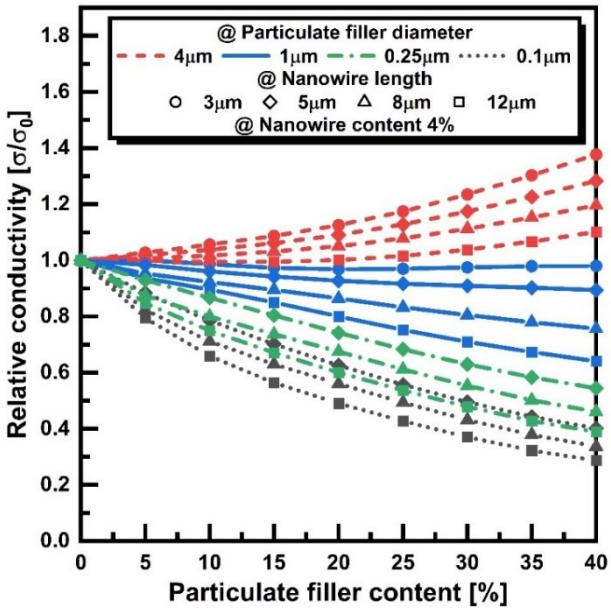

Figure 1. Relative electrical conductivity of the hybrid nanocomposite with respect to particulate filler concentrations under various configurations of particulate filler diameters and nanowire lengths. Detailed explanations of Figure 1 are described in Supplementary Note 1.

Fig. 1 shows the relative conductivity (σ/σ_0) of the hybrid nanocomposites, which is defined as the ratio of the electrical conductivity of the hybrid nanocomposites (σ) to the conductivity of composite materials with only a nanowire filler (σ_0) under various design parameters, including the particulate filler diameter (D), nanowire length (L), particulate filler concentration (P), and nanowire concentration (N). Monte Carlo-based numerical simulations for the comprehensive arrangement of these four parameters are conducted[19,20], and bootstrapping techniques are applied to the dataset for an extended set of parameter configurations[29]. The details of the method are provided in Supplementary Figure 1a. According to the data analysis shown in Fig. 1, the hybrid nanocomposite networks reveal distinct characteristics of abrupt transition

phenomena in the conductive properties, which are not observed in the single-type filler composite network. σ/σ_0 mainly depends on the combined properties of multiple design parameters rather than a change in a single parameter. To observe this more carefully, we use statistical analysis techniques to discriminate the dominant factor for the σ/σ_0.

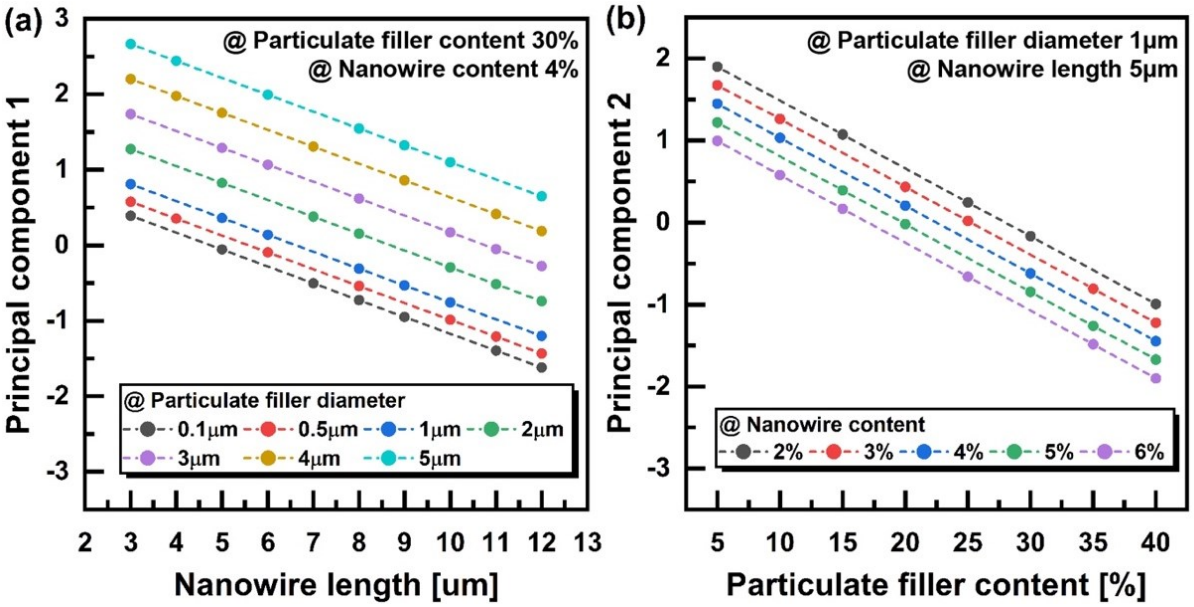

Figure 2. a Variation of principal component 1 with respect to the nanowire lengths for different particulate filler diameters at a particulate filler content of 30% and a nanowire filler content of 4%. **b** Variation of principal component 2 with respect to the particulate filler contents for different nanowire contents at a fixed particulate filler diameter of 1 μm and a nanowire length of 5 μm.

Principal component analysis (PCA) is employed over the space of design parameters D, L, P, and N to determine a subset of parameters that dominate σ/σ_0[30]. The PCA results indicate that the first two principal components (PCs) are sufficient to ensure a complete description of the space of the four design parameters. The determination of the relationship between the two PCs with a set of D, L, P, and N, illustrated in Figure 2, aims to justify the observation from the numerical simulation results shown in Fig. 1, implying that multiple physical parameters jointly determine the electrical properties

of hybrid nanocomposites. As shown in Figure 2a, the first PC (PC1) is proportional to D, while increasing L results in a linear decrease of the PC1 value. In addition, P and N are independent of PC1, as shown in Supplementary Fig. 2a and 2b. Figure 2b shows the relationships between the second PC (PC2). The PC2 value is inversely proportional to P and N and invariant with D and L (Supplementary Fig. 2c and 2d). These observations enable to model PC1 as a function that increases proportionally with the D/L ratio, whereas PC2 is considered a function of 1/(PN). This implies that σ/σ_0 can be characterized using a one-dimensional model under the condition that P and N are fixed.

2) Deep neural network-based computational models for the electrical conductivity

A functional model described with a single D/L parameter is optimized using a one-dimensional regressive model pursued using deep neural network (DNN) and statistical techniques. The resulting model is obtained in the form of a fractional function, as shown in equation (1). The set of numerical parameters associated with the model (e.g., A_1, A_2, p, and x_0) is configured for σ/σ_0 under various conditions for P and N. Supplementary Table 1 presents the configurations of the fitting parameters according to the condition set of P and N. The corresponding functional values are illustrated along with the computational data obtained from the numerical simulation in Figure 3.

$$\frac{\sigma}{\sigma_0} = A_2 + \frac{A_1 - A_2}{1 + \left(\frac{D}{x_0 L}\right)^p} \quad (1)$$

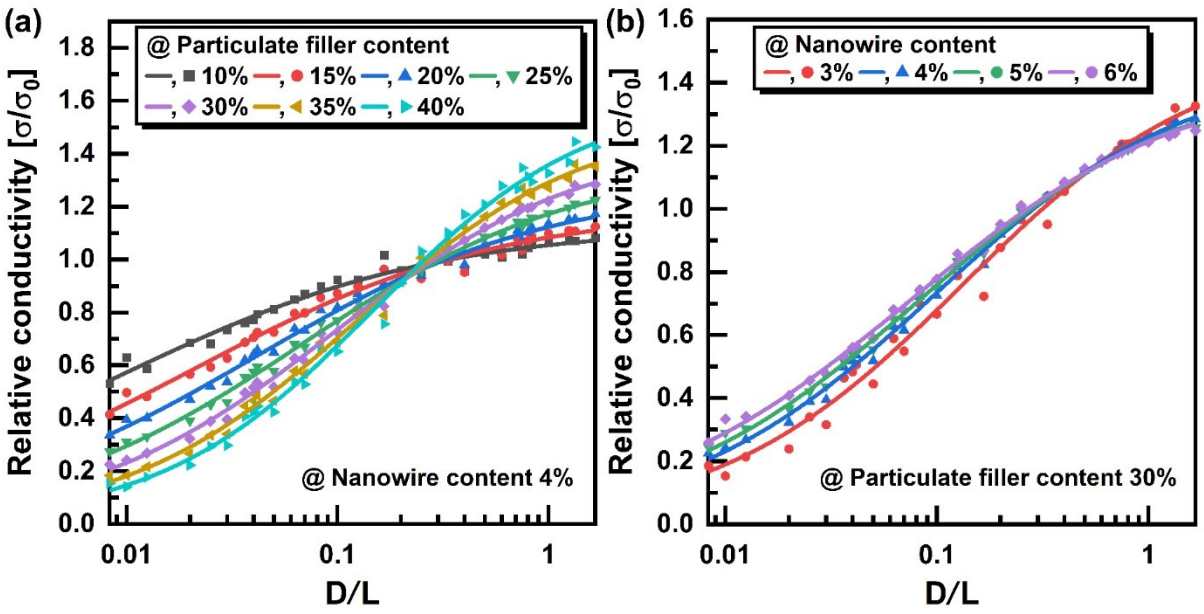

Figure 3. Tendencies of the relative electrical conductivity of hybrid nanocomposites with respect to D/L. The data obtained from equation (1) are plotted with solid lines, and the data from the numerical simulation appear as solid markers. Variation of the relative conductivities according to **a** the content of insulating particulate fillers; **b** the content of conducting nanowires.

According to Figure 3, σ/σ_0 increases as the D/L ratio increases for all content conditions. However, when the filler content is fixed, the electrical conductivity cannot increase without a bound nor take a negative value. Therefore, it is bounded below by a positive value as the D/L ratio decreases and above by a specific maximum value for the increasing ratio. Therefore, the corresponding function is expected to be a sigmoid function. Meanwhile, the conductivity variation rate of the change mainly depends on the combination of the two filler contents, as indicated by the change in the values of the fitting parameters associated with the conditions of P and N listed in Supplementary Table 1. Further details of the verification of the values of parameters A_1, A_2, and p of equation (1) listed in can be found in Supplementary Note 4.

3) Quantitative analysis of mechanism for the change of electrical conductivity

The analysis results presented in Supplementary Note 4 indicate that the variation in σ/σ_0 is attributed to the change in the morphology of the nanowire network caused by the particulate fillers and the corresponding change in the percolation probability. In other words, according to the relative dimensions of the particulate fillers with respect to the nanowires, the multifold phenomena of the exclusive volume effect and the nanowire bending effect compete to show distinct electrical properties. However, previous studies have only applied qualitative approaches and have failed to gain a comprehensive understanding of the two conflicting effects[19-20]. Therefore, this study aims to quantitatively characterize the effects to identify their extent according to D/L. Furthermore, an analytical model for these effects is investigated to evaluate the degree of importance of these conflicting effects in determining the percolation probability of the nanowire network in the hybrid nanocomposite. To achieve this goal, a set of representative parameters that describe and measure the effects in numerical values is carefully chosen, as described in Supplementary Note 5.

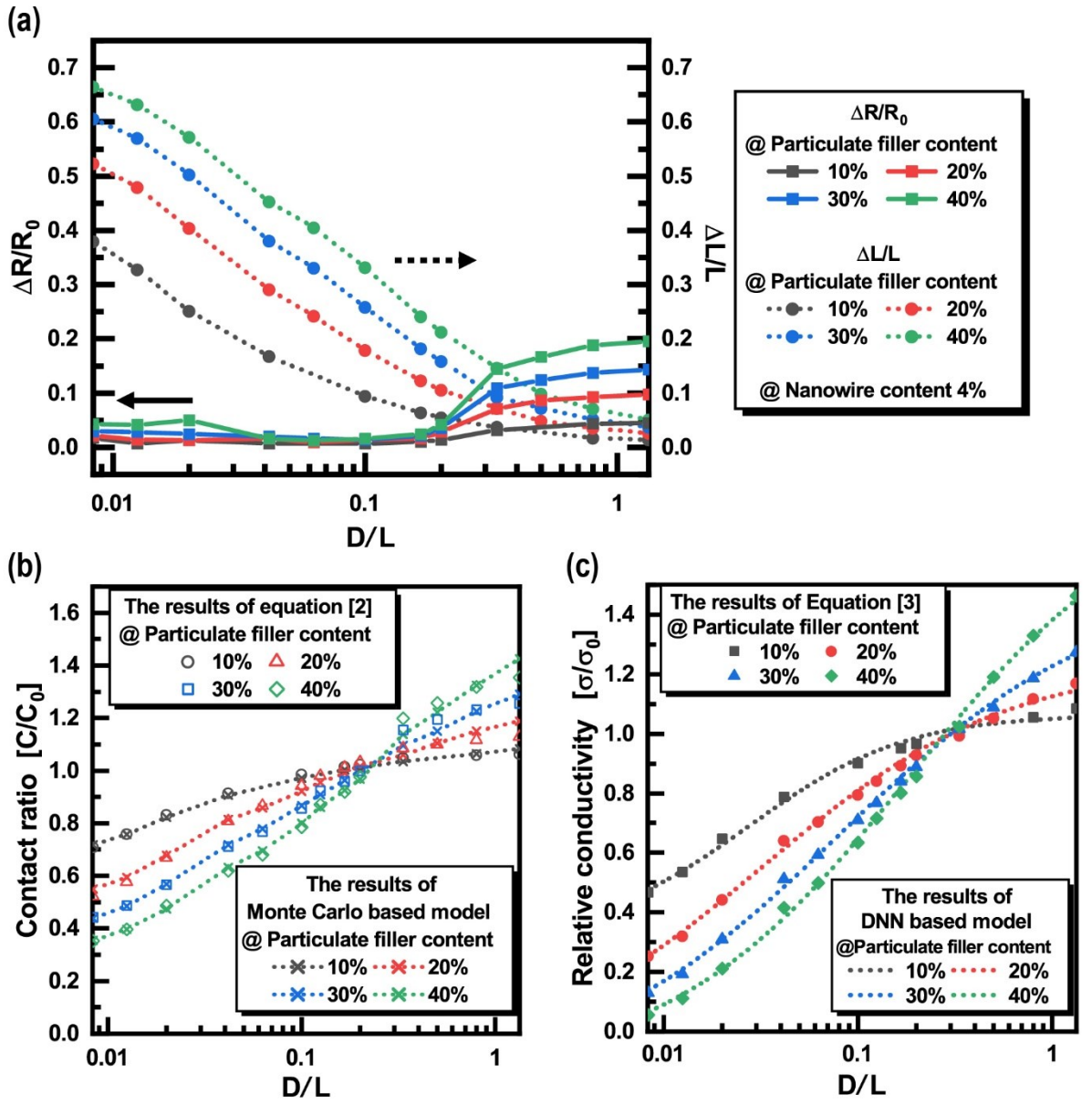

Figure 4. a Relative variation of the average nearest neighbor ratio of the center point of the nanowires ($\Delta R/R_0$) and effective nanowire length ($\Delta L/L$) with respect to D/L. **b** Ratio of the number of contacts in a nanowire network generated in the hybrid nanocomposite to that in the nanowire network without particulate fillers (C/C_0) with respect to D/L. Data appearing with open markers obtained from equation (2) are plotted simultaneously with the data generated by the Monte Carlo-based numerical simulations represented with dotted lines and cross markers. **c** Relative conductivity (σ/σ_0) obtained from equation (3) is plotted with solid markers, and that from DNN-based computational models with respect to D/L is plotted with dotted lines.

The first parameter is the relative variation in the average nearest neighbor ratio of the center point of the nanowires ($\Delta R/R_0$), representing the exclusive volume effect

resulting from particulate fillers. Figure 4a depicts the value of $\Delta R/R_0$ evaluated with respect to D/L, which increases with an upper limit as D/L becomes large. For a sufficiently large value of D/L, the exclusive volume effect becomes saturated because the concentration of the particulate filler is finite. Its upper limit value increases to accommodate the increasing content of particulate fillers. This results from the enhancement of the blockage of nanowire scattering by the increase in the region occupied by the particulate filler. In addition, the exclusive volume effect is negligible for small values of D/L, as shown in Supplementary Figure 3b; therefore, $\Delta R/R_0$ decays to zero. The second parameter represents the effective nanowire bending ($\Delta L/L$), and its value with respect to D/L is shown in Fig. 4a. In the case of a large D/L, nanowires can be located over a region without particulate fillers, so they tend to be straight, resulting in $\Delta L/L$ naturally approaching zero. However, in the case of a small D/L value, the nanowire is likely to be bent by several nearby particles, increasing $\Delta L/L$. With a fixed value of D/L, a large population of particulate fillers increases the number of neighboring fillers around the nanowire, increasing $\Delta L/L$.

To combine these two parameterized features of the exclusive volume effect and nanowire bending effect, a statistical technique based on linear regression is applied to obtain an expression that includes the arrangement of parameters required to describe the two effects. In particular, the percolation probability of nanowire networks is evaluated based on the ratio of the number of contacts observed in the hybrid nanocomposite networks (C) and nanowire networks without particulate fillers (C_0); that is, it is expressed in terms of a new parameter (C/C_0) using equation (2):

$$\frac{C}{C_0} = \alpha \times \frac{\Delta R}{R_0} + \beta \times \frac{\Delta L}{L} + \gamma \qquad (2)$$

Three numerical parameters—α, β, and γ—are introduced for this target. To be precise, α and β can be viewed as weight parameters that determine the contributions of the two effects based on the content of the fillers (P and N). In contrast, γ is a compensation coefficient that makes them commensurable and reflects other minor factors. Figure 4b shows the statistically processed data based on equation (2) and the value of the C/C_0 data obtained from the Monte Carlo-based numerical simulation.

Table **1** lists the important configurations of the parameters α, β, and γ for distinct conditions of P and N. The exclusive volume effect increases the percolation probability, which results in α with a non-negative value. In contrast, the bending effect reduces the percolation probability, leading to a negative value of β. These two effects strengthen if the content of the particulate fillers increases; therefore, the resulting parameters have large absolute values. The results imply that, in hybrid nanocomposites, particulate fillers induce a variation in these two effects based on the relative size of the two fillers (D/L). Their overall additive impact can be described in terms of the percolation probability of the nanowire network.

Table 1. Regression results of equation (2)

P [%]	N [%]	α	β	γ
10	4	0.0125	-0.9678	1.0751
20	4	0.0214	-1.2214	1.1583
30	4	0.9753	-1.2317	1.1608
40	4	1.0163	-1.3784	1.2256

Furthermore, a statistical technique based on logistic regression is conducted to determine the explicit relationship between the percolation probability of the nanowire network and the electrical conductivity of the hybrid nanocomposite material. The computational mapping yields σ/σ_0 from the value of C/C_0 associated with the

percolation probability in equation (3):

$$\frac{\sigma}{\sigma_0} = b_1 \left(\frac{C}{C_0}\right)^{b_2} + b_3 \quad (3)$$

Figure 4c plots the two results related to the value of σ/σ_0 obtained from the logistic regression and the DNN-based computational models discussed previously. The values of the fitting parameters b_1, b_2, and b_3 for several configurations of P and N are listed in Supplementary Table 2. The detailed explanation for these fitting parameters is described in Supplementary Note 5. The results demonstrate that the change of the percolation probability of the nanowire network caused by the particulate fillers has a critical role in the variation of σ/σ_0.

4) Voronoi-geometric characterization for electrical conductivity

The electrical conductivity of the hybrid nanocomposites is formulated in a computational model using numerical simulations and an analytical approach for dimensional reduction of the numerical results based on logistic regression. This model developed the relationship between the electrically conductive properties and geometric parameters of the nanowires and particulate fillers. In addition, it is verified that the morphological changes in the nanowire network induced by the content variation of particulate fillers and their associated percolating properties are major attributes of the fundamental mechanism of the change in electrical conductivity. Based on the results that have been presented so far, a qualitative understanding based on computational geometry is introduced by combining the concepts of Voronoi tessellation and Swiss cheese models to enhance quantitative characterization. This computational geometrical framework simplifies the essential structure of the filler

distribution and, subsequently, the topology of the nanowire networks generated in the hybrid nanocomposites. This essential topology of the nanowire network can also be further characterized by employing two important notions of effective density and tortuosity. To this end, the effective density and tortuosity are expressed in terms of the parameter D/L, which is critical for determining electrical conductivity. Through such a model, one-dimensional characterization of the electrical conductivity of the hybrid nanocomposites can be completed.

Fig. 5 presents the detailed procedure for developing the computational geometrical framework, in which the representative conducting paths in the nanowire network are defined and parameterized via the introduction of Voronoi tessellation. A detailed explanation of Figure 5 is provided in Supplementary Note 6. The model can be interpreted as a continuous percolating network of Voronoi edges. The nanowire network is integrated into each of the edges; therefore, the distribution of a nanowire bundle associated with an edge of Voronoi tessellation also affects the current flow through the conducting path. Thus, in addition to the neck width of each conducting path, the distribution of the underlying nanowires in the corresponding path has a critical impact on the conductivity of each conducting path.

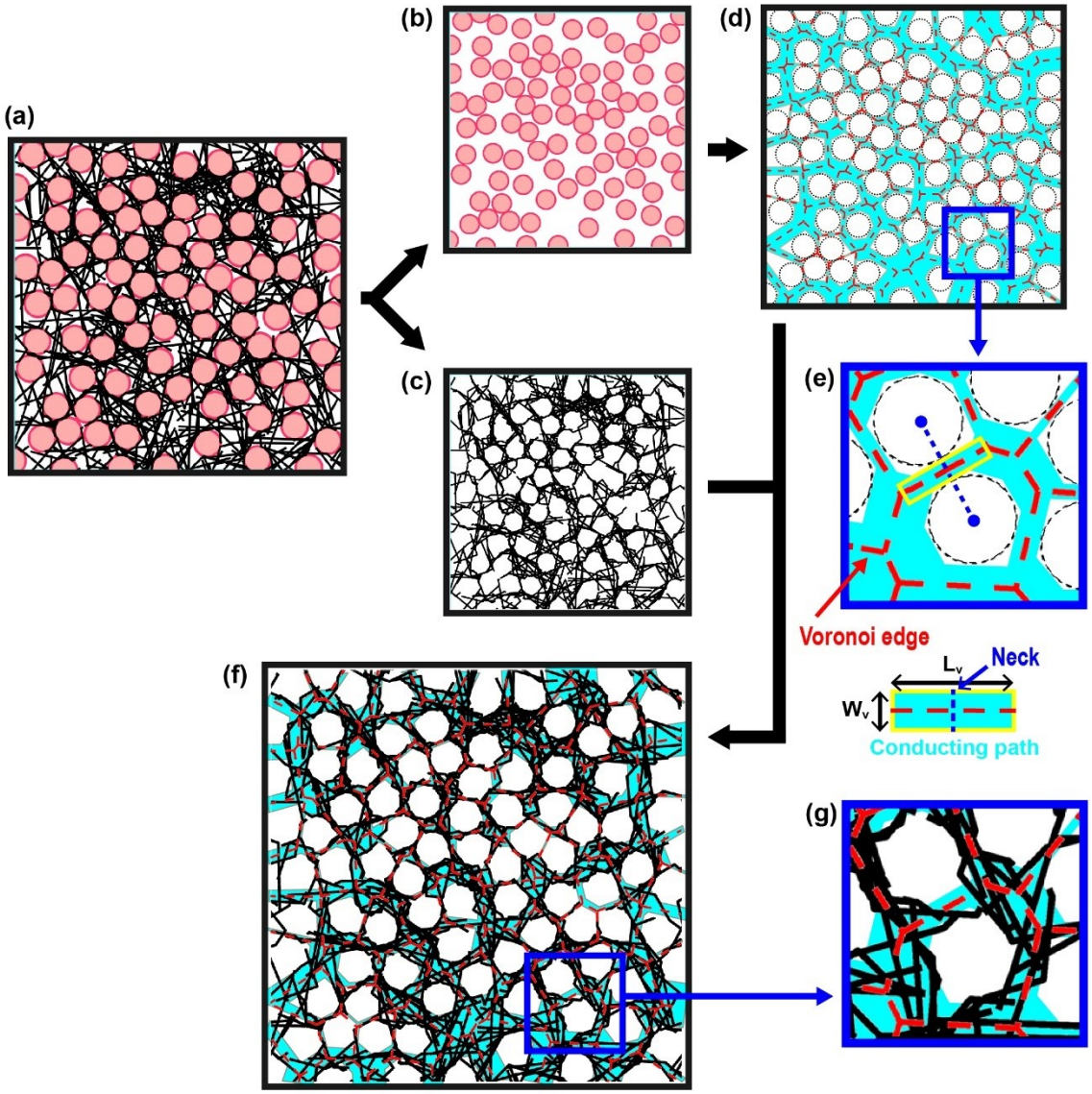

Figure 5. a Example of a hybrid nanocomposite. **b** Distribution of particulate fillers separated from 5a. **c** Distribution of nanowires separated from 5a. **d** Voronoi tessellation constructed based on the center point of particulate fillers in 5b, presented with red dashed lines. The corresponding conducting paths are indicated with cyan solid lines considering the neck widths. **e** Enlarged view of the region from 5d marked by a blue square. **f** Overlay of the nanowire network from 5c on the conducting paths from 5d and **g** magnified image of a region in 5f marked by a blue square.

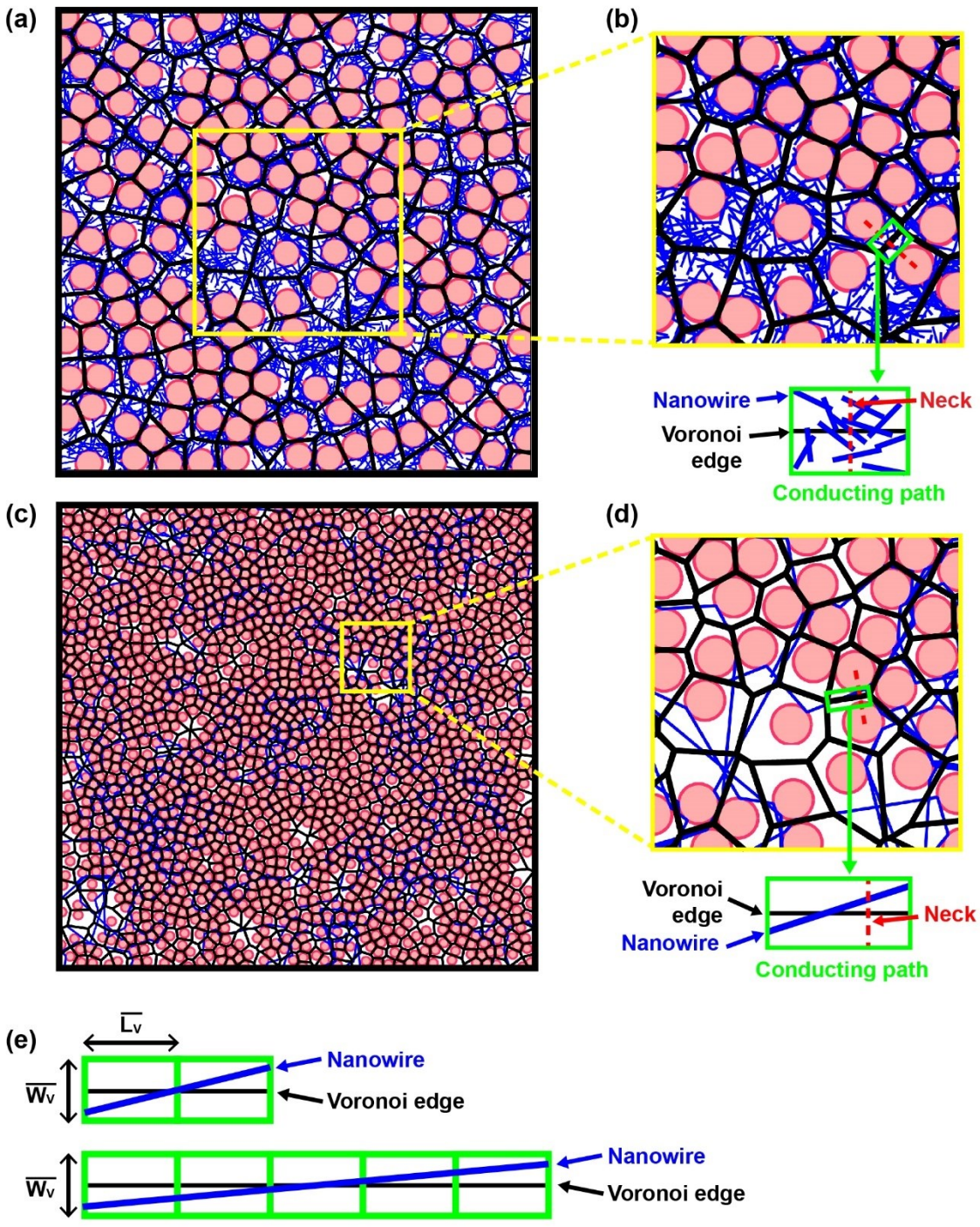

Figure 6. a Hybrid nanocomposite for the case of a large value of D/L and **b** the same nanocomposite drawn in the scaled simulation domain marked by the yellow square in 6a. **c** Hybrid nanocomposite for the case of a small value of D/L and **d** the same nanocomposite drawn in the scaled simulation domain marked by the yellow square in 6c. A Voronoi tessellation for each figure is represented by solid black lines. **e** Illustrations showing nanowires (solid blue lines) extended over the two (top) and five (bottom) adjacent conducting paths

Taking advantage of the computational geometrical framework, the conductivity of the hybrid nanocomposites can be further parameterized using the Voronoi geometry when P and N are fixed. Figure 6 depicts the hybrid nanocomposite networks with two distinct values of D/L but fixed values for P and N. Two cases of large and small values of D/L are presented in Figure 6a and 6c, respectively. If P is fixed, the Voronoi tessellation can be scaled regardless of D/L values based on the renormalization of parameters with an appropriate definition of the simulation domain. For example, Figure 6b shows the scaled simulation domain corresponding to the yellow square in Figure 6a, where the side length of the domain is 10 μm, and the value of D is 1 μm. In contrast, Figure 6d shows the scaled simulation domain represented by the yellow square in Figure 6c, in which the side length of the domain is 1 μm and the value of D is 0.1 μm. These two scaled simulation domains have Voronoi tessellations with the same connectivity; the two systems have the same conducting path configurations. Therefore, the difference in the electrical conductivities for the two distinct nanocomposite materials with different values of D/L, as shown in Figure 6b and 6d, depends on the difference of the conductivity associated with the individual conducting path. In addition, as ensemble averages generally determine the properties of random structures, the conductivity of hybrid nanocomposites can be characterized by the average conductivity of a single conducting path.

To derive the electrical conductivity of a conducting path induced by nanowire bundles incorporated into it, an underlying principle for the Kozeny–Carman approach is introduced, which was originally developed to describe the permeability (hydraulic conductivity) of a porous medium[31]. In this approach, when fluid flows across a porous medium, the hydraulic conductivity of the medium is proportional to the porosity of the medium and inversely proportional to the tortuosity of the path. In contrast to the Swiss

cheese model, in which the conducting path forms in a medium other than the pores, the fluid flows along the porous region in this approach. A high porosity implies a large conducting path width, helping the flow in the porous medium. In our model, current flows through a conducting path along the region occupied by the nanowires. Thus, a high density of nanowires placed along the conducting path corresponds to high porosity and increasing conductivity. Tortuosity is the average flow path length ratio to the sample length. A group of nanowires aligned parallel to the associated Voronoi edge improves the effective conductivity of the conducting path.

These properties can be incorporated into a single mathematical expression in equation (4). L, W_{NW}, and N_{NW} denote the length, width, and population of the nanowire in the simulation domain, respectively, N_{NP} is the population of the particulate filler in the simulation domain, and L_V and W_V represent the length and neck width of the conducting path, respectively, as shown in Fig. 5e. Because L_V and W_V vary with a gamma distribution[32] in a simulation domain where the particulate fillers are randomly distributed, their mean values ($\overline{L_V}$ and $\overline{W_V}$, respectively) are used for macroscopic evaluation of the conductive performance.

$$\frac{\sigma}{\sigma_0} = \frac{\left[\left(\frac{W_{NW}}{\overline{W_V}}\right) \times \left(\frac{N_{NW}}{3N_{NP} - 6}\right)\right]^{\omega}}{c_1\left[1 + \left(\frac{\overline{W_V}}{L} \times \frac{\overline{L_V}}{L}\right)^{\gamma}\right]} \tag{4}$$

The numerator in equation (4) corresponds to the average density of a collection of nanowires crossing the neck associated with a conducting path and can be addressed in terms of the porosity of the medium for the Kozeny–Carman approach. The number of Voronoi edges within the domain containing N_{NP} particulate fillers is approximately $3N_{NP}-6$. This indicates that the average number of nanowires crossing the neck becomes $N_{NW}/(3N_{NP}-6)$. The overall volume of the space occupied by a nanowire

bundle in a conducting path can be approximated by multiplying the population of the nanowire bundle with the nanowire width W_{NW}. If this quantity is divided by the neck width $\overline{W_V}$, the effective density of the nanowire bundle within the neck associated with the Voronoi edge is obtained. This corresponds to the volume density of the path in which the current flows, equivalent to the average porosity of the conducting path.

Furthermore, the denominator of equation (4) is associated with tortuosity of the current path, which is the extent of bending of the nanowires crossing the neck of a Voronoi edge. As the population of nanowires aligned with the Voronoi edge increases, the tortuosity of the current path decreases, implying an improvement in the conductivity of the conducting path. Figure 6b and 6d illustrate the distribution of nanowire bundles crossing the neck of the Voronoi edge. In the case of a large D/L ratio (Figure 6b), the neck width of the Voronoi edge was comparable to the nanowire length. Some nanowires of the nanowire bundle were distributed in a random direction rather than aligned in parallel with the Voronoi edge. In contrast, a small value of D/L (Figure 6d) allows the length of the nanowire to become considerably longer than the neck width; therefore, nanowires tend to align with the Voronoi edge in a parallel direction. Thus, the tortuosity of the current path along the conducting path can be considered proportional to $\overline{W_V}/L$. In addition, the ratio of the nanowire length to the average length of the Voronoi edge affects the tortuosity. Suppose the length is sufficiently long to allow a single nanowire to pass through multiple conducting paths. There is an increased chance that a nanowire in a conducting path is aligned parallel with the Voronoi edge. For example, as shown in Figure 6e, the nanowire approximately twice as long as $\overline{L_V}$ is less likely to be aligned to a Voronoi edge as compared to the nanowire approximately five times as long as $\overline{L_V}$. This indicates that the tortuosity of the current path formed by the nanowire bundle associated with a

conducting path is inversely proportional to the number of Voronoi edges that a single nanowire can cover, i.e., proportional to $\overline{\mathrm{L_V}}/L$. Thus, tortuosity is proportional to $(\overline{\mathrm{W_V}}/L) \times (\overline{\mathrm{L_V}}/L)$ in the denominator of equation (4). An additive constant of one is introduced to this quantity to model its gradual tendencies with the upper and lower limits such that the denominator is given by $1 + \left(\frac{\overline{W_V}}{L}\right) \times \left(\frac{\overline{L_V}}{L}\right)$.

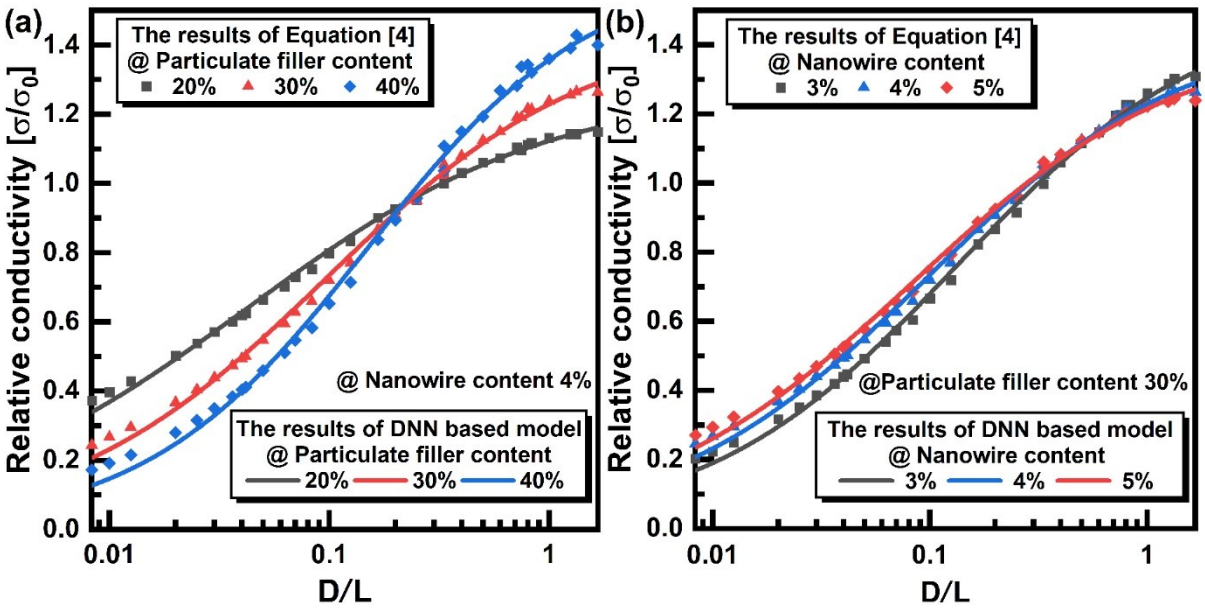

Figure 7. Relative electrical conductivity of hybrid nanocomposites with respect to D/L. The data appearing with solid markers obtained from equation (4) are plotted simultaneously with the data obtained from DNN-based computational models presented with solid lines. **a** Variation of the relative conductivities according to the content of insulating particulate fillers. **b** Variation of relative conductivities according to the content of conducting nanowires.

Table 2. Regression results of equation (4)

P [%]	N [%]	ω	γ	c_1
20	4	0.3850	0.3118	0.1240
30	4	0.4825	0.4204	0.0912
40	4	0.5629	0.5438	0.0722
30	3	0.5272	0.4298	0.0668
30	4	0.4825	0.4204	0.0912
30	5	0.4583	0.4194	0.1104

To address the impact of parameters P and N on equation (4), an additional arrangement of parameters ω, γ, and c_1 is introduced. The change in σ/σ_0 is obtained using statistical techniques based on logistic regression for various configurations of P and N. In Figure 7, the obtained model is plotted together with the results from the DNN-based model discussed in the previous section, showing that the analytical relationship can accurately express the change in electrical conductivity of the hybrid nanowire network. Table 2 lists the arrangement of the parameters determined by the regression. The exponents of the porosity and tortuosity, described by ω and γ, respectively, become significant when the particulate filler content increases with respect to the nanowire content, for an increasing P/N ratio. This indicates that the topological variation in the porosity and tortuosity of the nanowire network caused by the particulate fillers has a more critical impact on the transition of the electrical conductivity of the hybrid nanocomposite. Concerning the last parameter, c_1, its value decreases as the P/N ratio increases. This can be viewed as a decrease in the proportional constant of the denominator in equation (4), which resulted from an increase in the particulate filler content. Therefore, the proportionality constant in equation (4) increases with P/N, implying that the range of the σ/σ_0 variation increases with particulate filler content.

Discussion

Parameters $\overline{L_V}$ and $\overline{W_V}$ in equation (4) were determined from the random distribution model of the particulate filler constructed by the Monte Carlo simulation, as shown in Figure 5d. This study aims to develop an analytical model to describe the electrical conductivity of hybrid nanocomposites based on the design parameters D, L, P, and N to readily design composite materials with the desired characteristics before material fabrication. Hence, $\overline{L_V}$ and $\overline{W_V}$ in equation (4) are substituted into the analytical equations, $\overline{L_V} = \frac{2}{3\sqrt{\lambda}}$ and $\overline{W_V} = \frac{32}{9\pi\sqrt{\lambda}} - D$, as given in Refs. 33 and 34, respectively, where λ is the intensity of the planar Poisson points. As the number of particulate fillers is equal to λ times the area of the simulation domain, λ is a function of D and P; thus, $\overline{L_V}$ and $\overline{W_V}$ can be replaced by functions of the design parameters. The steps for deriving the expressions for $\overline{L_V}$ and $\overline{W_V}$ are outlined in Supplementary Note 7. To verify the validity of the formulas, the values of $\overline{L_V}/D$ and $\overline{W_V}/D$ calculated from the analytic expressions versus P and Monte Carlo simulation are plotted in Supplementary Fig. 6a and 6b, respectively.

Furthermore, the $\left(\frac{N_{NW}}{3N_{NP}-6}\right)$ term in the numerator of equation (4) can be replaced by the function with respect to the design parameters by ignoring the number 6 of the denominator negligibly small as compared to the values of N_{NW} and N_{NP}. The detailed procedure for the derivation of the analytic expression is provided in Supplementary Note 9. By replacing $\overline{L_V}$, $\overline{W_V}$, N_{NW}, and N_{NP} in equation (4) with the functions of the design parameters D, L, P, and N, respectively, the analytical model in terms of the design parameters can be expressed as follows:

$$\frac{\sigma}{\sigma_0} = \frac{C_1 \left(\frac{D}{L}\right)^{\omega}}{1 + C_2 \left(\frac{D}{L}\right)^{2\gamma}} \quad (5)$$

where $C_1 = \frac{1}{c_1}\left(\frac{\pi N}{12P}\right)^{\omega}\left(\frac{16}{9\sqrt{\pi P}} - 1\right)^{-\omega}$ and $C_2 = \left(\frac{\sqrt{\pi}}{3\sqrt{P}}\right)^{\gamma}\left(\frac{16}{9\sqrt{\pi P}} - 1\right)^{\gamma}$. equation (5) becomes a one-dimensional function of the variable D/L under the condition of fixed values of P and N, as suggested from previous results obtained by DNN techniques. Employing the values of ω, γ, and c_1 listed in Table 2, the σ/σ_0 values were evaluated from equation (5). The results are plotted in Supplementary Fig. 7a and 7b, together with those obtained from the Monte Carlo simulation, demonstrating a good agreement.

Equation (5) is not a monotonically increasing function with upper and lower bounds, as in the case of equation (1) derived from the DNN model; however, it is a function that initially increases to its maximum value with its subsequent decrease. Therefore, equation (5) is valid in the range of D/L from 0 to $(D/L)_{max}$, at which σ/σ_0 reaches the maximum value, $(\sigma/\sigma_0)_{max}$, and σ/σ_0 remains constant at the maximum value when D/L is higher than $(D/L)_{max}$. The values of $(D/L)_{max}$ and $(\sigma/\sigma_0)_{max}$ are associated with the variables P and N as well as the fitting parameters of ω, γ, and c_1, as presented in Supplementary Note 9. When the $(\sigma/\sigma_0)_{max}$ values are estimated with the fitting parameters listed in Table 2, they are smaller than the values of A_2 presented in Supplementary Table 1, which corresponds to the maximum value of equation (1) because the values of ω, γ, and c_1 are obtained by fitting data including $\overline{L_V}$ and $\overline{W_V}$ generated from the Monte Carlo simulation. Therefore, as listed in Supplementary Table 4, the ω, γ, and c_1 values are updated by regression using equation (5) with the analytic terms of $\overline{L_V}$ and $\overline{W_V}$, and thereby, comparable $(\sigma/\sigma_0)_{max}$ values with the value of A_2 can be attained with the modified ω, γ, and c_1 values, as provided in

Supplementary Table 5. The σ/σ_0 values of the hybrid nanocomposites are evaluated using equation (5). The evaluation values with revised fitting parameters and results from the Monte Carlo simulation are plotted in Supplementary Fig. 7c and 7d. Further investigation is required to substitute for ω, γ, and c_1 as fitting parameters with the explicit functions of the variables P and N to develop a comprehensive and precise model.

Conclusion

An analytical model for the electrical conductivity of the hybrid nanocomposites as a one-dimensional function of D/L is developed based on the geometrical framework, including the Voronoi tessellation and Swiss cheese model. The primary factor, D/L, which determines the electrical characteristics of nanocomposite materials, is identified by employing PCA and DNN. In addition, quantitative analysis reveals that the morphology change of the nanowire network due to the exclusive volume and nanowire bending effect originating from the distribution of the particulate fillers is the primary mechanism for the change in the electrical conductivity of the hybrid nanocomposites. Voronoi tessellation and the Swiss cheese model are employed to concisely describe the distribution of the particulate fillers. On the geometrical framework, the morphology of the nanowire network can be described using effective density and tortuosity as adopted by the Kozeny–Carman approach. The analytic model for σ/σ_0 of the hybrid nanocomposites with respect to the variable D/L is derived using these methodologies. The results calculated from the analytic expression closely match the numerical data, demonstrating the validity of the analytic expressions.

Methods

Long-short term memory-based model for data bootstrapping

A Monte Carlo-based numerical simulation requires high computational cost and time for a comprehensive evaluation of the electrical properties of the hybrid nanocomposite. To overcome these limitations, the bootstrapping technique is applied to the dataset using the long-short term memory (LSTM) algorithm. This model is implemented using TensorFlow library[35] in Python 3.7. The LSTM-based model is composed of a four-input layer, and a single LSTM layer consisted of 30 units of memory cells, as shown in Supplementary Fig. 1a. The mean square error is applied to the cost function. LSTM-based supervised learning is used to predict the electrical conductivity of the hybrid nanocomposites under various conditions of D, L, P, and N.

PCA for low-dimensional characterization

PCA was designed in Python 3.7, using the open-source library scikit-learn[36]. The dataset for PCA consisted of two-dimensional tabular data with respect to the conditions of the constituent fillers. The labels in each column are D, L, P, and N; therefore, each row corresponds to the set of design parameters required to generate a random instance of the hybrid nanocomposite. The labels in each row represent the relative conductivities of the hybrid nanocomposites. Dimension reduction is performed on the dataset using PCA.

DNN-based regression model

A DNN-based regression model is implemented in Python 3.7, and the fundamental

layers for the DNN in this model are constructed using the open-source library TensorFlow[35]. The DNN-based regression model consisted of two sub-models. The first sub-model employs DNN as a regression model, in which curves are regressed by linking adjacent points with small line segments with respect to D/L at fixed values of P and N. The DNN-based model consisted of a single input layer and five dense layers, as shown in Supplementary Fig. 1b. The second sub-model is a linear and nonlinear regression model with 22 basis functions, including polynomial, exponential, trigonometric, and other mathematical functions in the TensorFlow library[35]. The first and second sub-models are merged, and the regression model is trained to minimize the mean square error between the results of the first and second regression models.

Acknowledgment

This work was supported by the National Research Foundation of Korea (NRF) grant funded by the Korea government. (MSIT) (No. 2021R1C1C1014146).

References

1 Sharif, F., Arjmand, M., Moud, A. A., Sundararaj, U. & Roberts, E. P. L. Segregated Hybrid Poly(methyl methacrylate)/Graphene/Magnetite Nanocomposites for Electromagnetic Interference Shielding. *ACS Applied Materials & Interfaces* **9**, 14171-14179, doi:10.1021/acsami.6b13986 (2017).

2 Uddin, M. F. & Sun, C. T. Improved dispersion and mechanical properties of hybrid nanocomposites. *Composites Science and Technology* **70**, 223-230, doi:https://doi.org/10.1016/j.compscitech.2009.09.017 (2010).

3 Kim, D., Kim, Y., Choi, K., Grunlan, J. C. & Yu, C. Improved Thermoelectric Behavior of Nanotube-Filled Polymer Composites with Poly(3,4-ethylenedioxythiophene) Poly(styrenesulfonate). *ACS Nano* **4**, 513-523, doi:10.1021/nn9013577 (2010).

4 Xing, G. Z. *et al.* Hybrid CuO/SnO2 nanocomposites: Towards cost-effective and high performance binder free lithium ion batteries anode materials. *Applied Physics Letters* **105**, 143905 (2014).

5 Jahan, N., Mighri, F., Rodrigue, D. & Ajji, A. Synergistic improvement of piezoelectric properties of PVDF/CaCO3/montmorillonite hybrid nanocomposites. *Applied Clay Science* **152**, 93-100 (2018).

6 Fathy, A., Abu-Oqail, A. & Wagih, A. Improved mechanical and wear properties of hybrid Al-Al2O3/GNPs electro-less coated Ni nanocomposite. *Ceramics International* **44**, 22135-22145 (2018).

7 Yao, Q., Chen, L., Zhang, W., Liufu, S. & Chen, X. Enhanced thermoelectric performance of single-walled carbon nanotubes/polyaniline hybrid nanocomposites. *Acs Nano* **4**, 2445-2451 (2010).

8 Ulus, H. *et al.* Boron nitride-MWCNT/epoxy hybrid nanocomposites: Preparation and mechanical properties. *Applied Surface Science* **318**, 37-42 (2014).

9 de Andrade, M. J. *et al.* Electrical conductive double-walled carbon nanotubes–Silica glass nanocomposites prepared by the sol–gel process and spark plasma sintering. *Scripta Materialia* **61**, 988-991 (2009).

10 Sivakumar, R., Guo, S., Nishimura, T. & Kagawa, Y. Thermal conductivity in multi-wall carbon nanotube/silica-based nanocomposites. *Scripta Materialia* **56**, 265-268 (2007).

11 Kong, L. *et al.* High-performing multi-walled carbon nanotubes/silica nanocomposites for elastomer application. *Composites Science and Technology* **162**, 23-32 (2018).

12 Subhani, T. *et al.* Mechanical performance of epoxy matrix hybrid nanocomposites containing carbon nanotubes and nanodiamonds. *Materials & Design* **87**, 436-444 (2015).

13 Wei, Y. *et al.* ZnO nanorods/Au hybrid nanocomposites for glucose biosensor. *Biosensors and Bioelectronics* **26**, 275-278 (2010).

14 Weber, M. & Kamal, M. R. Estimation of the volume resistivity of electrically conductive composites. *Polymer composites* **18**, 711-725 (1997).

15 Lu, W., Chou, T.-W. & Thostenson, E. T. A three-dimensional model of electrical percolation thresholds in carbon nanotube-based composites. *Applied Physics Letters* **96**, 223106 (2010).

16 Jung, S. *et al.* Modeling electrical percolation to optimize the electromechanical properties of CNT/polymer composites in highly stretchable fiber strain sensors. *Scientific reports* **9**, 1-10 (2019).

17 Minelli, M., Baschetti, M. G. & Doghieri, F. A comprehensive model for mass transport properties in nanocomposites. *Journal of membrane science* **381**, 10-20 (2011).

18 Shady, E. & Gowayed, Y. Effect of nanotube geometry on the elastic properties of nanocomposites. *Composites Science and Technology* **70**, 1476-1481 (2010).

19 Park, S.-H. *et al.* Modeling the electrical resistivity of polymer composites with segregated structures. *Nature communications* **10**, 1-11 (2019).

20 Lee, J., Yun, Y., Lee, S. H. & Hwang, J. Numerical Characterization for Electrical Conductivity of Two-Dimensional Nanocomposite Systems with Conducting Fiber Fillers. *Materials* **13**, 2410 (2020).

21 Nam, I. W., Choi, J. H., Kim, C. G. & Lee, H.-K. Fabrication and design of electromagnetic wave absorber composed of carbon nanotube-incorporated cement composites. *Composite Structures* **206**, 439-447 (2018).

22 Kim, H. K., Nam, I. W. & Lee, H.-K. Enhanced effect of carbon nanotube on mechanical and electrical properties of cement composites by incorporation of silica fume. *Composite Structures* **107**, 60-69 (2014).

23 Palza, H., Garzón, C. & Arias, O. Modifying the electrical behaviour of polypropylene/carbon nanotube composites by adding a second nanoparticle and by annealing processes. *Express Polym. Lett* **6**, 639-646 (2012).

24 Park, S.-H. & Ha, J.-H. Improved electromagnetic interference shielding properties through the use of segregate carbon nanotube networks. *Materials* **12**, 1395 (2019).
25 Chen, Y.-F. *et al.* Achieving highly electrical conductivity and piezoresistive sensitivity in polydimethylsiloxane/multi-walled carbon nanotube composites via the incorporation of silicon dioxide micro-particles. *Composites Science and Technology* **177**, 41-48 (2019).
26 Xiong, Z.-Y., Zhang, B.-Y., Wang, L., Yu, J. & Guo, Z.-X. Modeling the electrical percolation of mixed carbon fillers in polymer blends. *Carbon* **70**, 233-240 (2014).
27 Pang, H., Xu, L., Yan, D.-X. & Li, Z.-M. Conductive polymer composites with segregated structures. *Progress in Polymer Science* **39**, 1908-1933 (2014).
28 Jin, L. *et al.* Microstructural origin of resistance–strain hysteresis in carbon nanotube thin film conductors. *Proceedings of the National Academy of Sciences* **115**, 1986, doi:10.1073/pnas.1717217115 (2018).
29 Lin, K., Peng, J., Gu, F. L. & Lan, Z. Simulation of Open Quantum Dynamics with Bootstrap-Based Long Short-Term Memory Recurrent Neural Network. *The Journal of Physical Chemistry Letters* **12**, 10225-10234, doi:10.1021/acs.jpclett.1c02672 (2021).
30 Wold, S., Esbensen, K. & Geladi, P. Principal component analysis. *Chemometrics and Intelligent Laboratory Systems* **2**, 37-52, doi:https://doi.org/10.1016/0169-7439(87)80084-9 (1987).
31 Ozgumus, T., Mobedi, M. & Ozkol, U. Determination of Kozeny Constant Based on Porosity and Pore to Throat Size Ratio in Porous Medium with Rectangular Rods. *Engineering Applications of Computational Fluid Mechanics* **8**, 308-318, doi:10.1080/19942060.2014.11015516 (2014).
32 Tanemura, M. Statistical distributions of Poisson Voronoi cells in two and three dimensions. *FORMA-TOKYO-* **18**, 221-247 (2003).
33 Muche, L. The Poisson-Voronoi tessellation: relationships for edges. *Advances in Applied Probability* **37**, 279-296, doi:10.1239/aap/1118858626 (2005).
34 Chang, R. C. & Lee, R. C. T. On the average length of Delaunay triangulations. *BIT Numerical Mathematics* **24**, 269-273, doi:10.1007/BF02136025 (1984).
35 Abadi, M. *et al.* Tensorflow: Large-scale machine learning on heterogeneous distributed systems. *arXiv preprint arXiv:1603.04467* (2016).
36 Pedregosa, F. *et al.* Scikit-learn: Machine learning in Python. *the Journal of machine Learning research* **12**, 2825-2830 (2011).

Supplementary Files

This is a list of supplementary files associated with this preprint. Click to download.

- SupplementaryInformationmanuscript.pdf